Adsorption of Acacia Gum on Self-Assembled Monolayer Surfaces: A Comprehensive Study Using QCM-D and MP-SPR

Athénaïs Davantès, Michael Nigen, Christian Sanchez, Denis Renard

HAL Id: hal-04681610
https://hal.inrae.fr/hal-04681610v1

Submitted on 29 Aug 2024

Adsorption of *Acacia* Gum on Self-Assembled Monolayer Surfaces: A Comprehensive Study Using QCM-D and MP-SPR

Athénaïs Davantès, Michaël Nigen, Christian Sanchez, and Denis Renard*

ACCESS | Metrics & More | Article Recommendations | Supporting Information

ABSTRACT: The interfacial structuring of *Acacia* gum at various pH values on self-assembled monolayer (SAM) surfaces was investigated in order to evaluate the respective importance of surface versus biopolymer hydration in the adsorption process of the gum. To this end, SAMs with four different ending chemical functionalities ($-CH_3$, $-OH$, $-COOH$, and $-NH_2$) were used on gold surfaces, and the gum adsorption was monitored using multiparametric surface plasmon resonance (MP-SPR) and quartz crystal microbalance with dissipation. Surface modification with alkanethiol and the subsequent adsorption of *Acacia* gum were also characterized by contact angle measurements using both sessile drop and captive bubble methods. According to MP-SPR results, this study demonstrated that gum adsorbed on all surfaces and that adsorption is the most favorable at both acid pH and hydrophobic environments, i.e., when both the surface and the biopolymer are weakly hydrated and more prone to interfacial dehydration. These results reinforce our recent proposal of interfacial dehydration-induced structuring of biopolymers. Increasing the pH logically decreased the adsorption capacity, especially on a hydrophilic surface, enhancing the hydration rate of the layer. A hydrophilic surface is unfavorable to *Acacia* gum adsorption except if the surface presents a negative surface charge. In this case, interfacial charge dehydration was promoted by attractive electrostatic interactions between the surface and biopolymers. In the aggregate, the water percentage and the viscoelastic properties were closely related to the properties of the surface function: the negative charge and hydrophobicity significantly increased the hydration rate and viscoelastic properties with the pH, while the positive charge induced a rigid and more dehydrated layer.
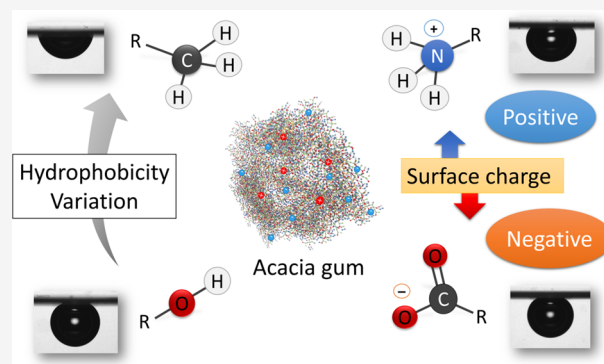
INTRODUCTION

The adsorption between biopolymers and solid surfaces plays a pivotal role in a multitude of scientific and industrial applications, ranging from pharmaceuticals to food science, but also environment and biomaterials.[1−6] Understanding the adsorption behavior of biopolymers, such as *Acacia* gum, on surfaces with varying properties, is of paramount importance as it not only contributes to our fundamental knowledge of interfacial phenomena but also finds practical relevance in numerous technological advancements. Self-assembled monolayers (SAMs) serve as a versatile platform to study adsorption due to their precise control over surface properties, including hydrophobicity, hydrophilicity, and charge, mimicking real-world scenarios.

Acacia gum, a complex highly branched arabinogalactan-protein (AGP) extracted from *Acacia* tree exudates, is widely used in food and pharmaceutical industries as a stabilizing, thickening, and gelling agent.[7,8] *Acacia* gums differ by their chemical composition, molecular weight distribution, protein content (∼1−3%), and composition in minor compounds (minerals, polyphenols).[8] Basically, AGPs are composed of protein backbones decorated with massive polysaccharide blocks.[9] Several previous studies have investigated the adsorption of *Acacia* gum on solid surfaces, like gold, oxide, or latex particles.[10−13] These studies highlighted that the adsorption of *Acacia* gum is the highest on hydrophobic and negatively charged surfaces, resulting in highly viscoelastic hydrated layers. Considering liquid oil−water interfaces, Faucon et al.[14] suggested that the dehydration of the interface, i.e., signature of surface hydrophobicity, is responsible for the gum adsorption near the oil hydrophobic interface. Furthermore, a recent study shows using in situ ATR-FTIR that *Acacia senegal* gum (*A. senegal*) adsorbs directly through the protein moieties on gold nanoparticle surfaces, while the carbohydrate blocks responsible for the high swelling capacity of the gum seem to be farther away from the interface.[15] However, most of these results were obtained on native and heterogeneous surfaces with no direct control over the surface charge or

hydrophobicity, two parameters that are intimately related. One possible route is to use well-defined and homogeneous surface chemistry such as SAMs of alkanethiolates with different ending chemical groups on gold surfaces. The adsorption of *Acacia* gum on SAM surfaces can be influenced by several factors, including the chemical composition and structure of the SAMs, as well as the pH and the ionic strength of the solution, to name a few. Several studies have investigated the influence of surface charge and wettability on the adsorption mechanism of proteins,[16−20] polymers,[21] bacteria,[22] or polysaccharides[23−25] using SAMs combined with QCM-D, SPR, and/or contact angle measurements.

In this study, we explore the adsorption behavior of *Acacia senegal* gum (*A. senegal*) on SAM surfaces with differing polarities (hydrophobic, polar, charged) at three different pH conditions using quartz crystal microbalance with dissipation (QCM-D) and multiparametric surface plasmon resonance (MP-SPR). QCM-D and MP-SPR are employed to investigate the adsorption amount, the hydration rate, and the viscoelastic properties of the adsorbed layers, providing a comprehensive overview of the adsorption process. Contact angle measurements, in both sessile drop (SD) and captive bubble (CB), are used to evaluate the impact of the gum on surface wettability in both air and buffer. By elucidating the interfacial interactions between *Acacia* gum and these diverse SAMs, we aim to shed light on the driving events governing this adsorption.

The findings of this study will not only advance our understanding of biopolymer-surface adsorption but also contribute to the development of improved *Acacia* gum-based formulations for diverse industrial applications. Furthermore, this research provides a valuable template for exploring the adsorption behavior of other biopolymers on structured surfaces, facilitating the design and optimization of advanced biomaterials and functional coatings.

■ EXPERIMENTAL SECTION

Materials. 1-Octadecanethiol (UDT: −CH$_3$, 98%), 11-mercapto-1-undecanol (MUD: −OH, 97%), 11-mercaptoundecanoic acid (MUA: −COOH, 95%), and 11-amino-1-undecanethiol hydrochloride (AUT: −NH$_2$, 97%) were all purchased from Sigma-Aldrich company. Ethanol absolute solution (99%) was purchased from Fisher Scientific.

The experiments were carried out using commercially available *Acacia senegal* (*A. senegal*, lot OF152413) soluble powders, provided by the Alland & Robert Company − Natural and Organic Gums (Port Mort, France). Biochemical composition and structural parameters are provided in the Supporting Information (Table S1). Dilution of stock gum dispersions (C = 10 g L^{-1}) to the desired concentrations was performed in 10 mM acetate (VWR Chemicals) with 50 mM NaCl salt. Gum concentrations in stock dispersions were quantified by the dry matter method. pH was set from 3 to 8 using HCl or NaOH solution (Merck, analytical grade, Molsheim, France). All stock solutions were prepared at room temperature and filtered with a 0.2 μm filter unit (GHP, Life Science), using fresh purified water (Milli-Q, Millipore) with a resistivity of 18.2 MΩ cm.

SAM Preparation and Cleaning. Gold substrates (QCM sensors and MP-SPR chips) were cleaned in piranha solution H$_2$SO$_4$/H$_2$O$_2$ (7:3, v/v) for 3 min, rinsed exhaustively first with Milli-Q water and then with absolute ethanol, and dried under a stream of nitrogen. SAMs were formed by immersing gold substrates into 2 mM thiol solutions in absolute ethanol overnight (∼18 h) at room temperature in the dark. Substrates were rinsed twice with absolute ethanol and dried under N$_2$. SAMs were kept away from light before contact angle analysis and after the adsorption experiment. After adsorption experiments, all substrates were rinsed thoroughly with Hellmanex 2%, ethanol, and water before recleaning with piranha solution.

MP-SPR. MP-SPR experiments were carried out on an MP-SPR Navi 210A VASA (BioNavis, Tampere, Finland). The wide angular range of 40°−78° available and the use of two wavelengths (670 and 785 nm) allow the direct determination of layer thickness and refractive index. An equilibration of 1−2 h with the buffer solution at the desired pH condition was needed to reach a stable state, corresponding to the baseline conditions. Considering the isotherm result obtained in our previous study, a concentration of 150 ppm was chosen for *A. senegal* adsorption in both MP-SPR and QCM-D experiments, corresponding to the maximum coverage concentration.[10] When the gum adsorption reached steady state, desorption was investigated by rinsing the system with an initial buffer solution.

The Navi LayerSolver software was used for the determination of the refractive index, thickness, and mass of the adsorbed gum using both wavelengths. For SAM film thickness determination, two different media (air and buffer) were also used combined with the two wavelengths. The following equation was used to calculate the adsorbed mass:

$$\Gamma_{MP-SPR} = d_{MP-SPR}*\rho \tag{1}$$

The film density was assumed to be the inverse of the partial specific volume v_s°, $\rho = 1/(v_s^\circ)$,[26] i.e., 1.703 cm^3 g^{-1}. The temperature was set to 20 °C with a flow rate of 50 μL.min^{-1}. All experiments were repeated at least twice, and all calculated data presented in this study corresponded to the mean ± standard deviation.

QCM-D Monitoring. The adsorption process was monitored in situ by QCM-D using a Q-sense E4 instrument (Sweden) using a piezoelectric AT-cut quartz crystal coated with gold electrodes, with a nominal resonance frequency of 5 MHz (SX301, Q-Sense) and a peristaltic pump to maintain the flow of the liquid through the measurement chamber. The detailed principles of the QCM-D method have been described elsewhere.[27,28] Briefly, by recording changes in the resonance frequency (Δ*F*) and the change in the dissipation energy (Δ*D*), this method allows the investigation of the mass change, the layer thickness, the kinetics of the adsorption process, and the viscoelastic properties of the adsorbed layer. The experimental process is identical to our previous study at 20 °C with a flow rate of 200 μL/min in an independent closed-system configuration for each cell.[13] As for MP-SPR, when the gum adsorption reached the steady state, desorption was investigated by rinsing the system with an initial buffer solution.

In this study, the Voigt model[29−31] was used to evaluate the mass, thickness, and viscoelastic properties of the adsorbed layer with the Dfind software with at least five overtones with a good signal-to-noise ratio (Biolin Scientific, Q-Sense, Sweden). The adsorbed film was assumed to have both a uniform thickness and a uniform density. All experiments were conducted at least three times. The ninth overtone presenting the best signal-to-noise ratio was used for data representation.

By comparing the "dry" mass from MP-SPR and the "wet" mass results from QCM-D, it is possible to estimate the apparent hydration rate of the adsorbed film according to the following equation:

$$\%H_2O = \frac{\Gamma_{QCM-D} - \Gamma_{MP-SPR}}{\Gamma_{QCM-D}}*100 \tag{2}$$

Contact Angle Measurement. Contact angle measurements were performed using two different methods: SD or CB, with a Tracker automatic drop tensiometer (Teclis Scientific). Images were analyzed with WDROP software.

SD contact angle measurements were performed by the method of SD. A drop of 2 μL of 10 mM acetate buffer containing 50 mM NaCl at the desired pH was deposited on the cleaned sensor surface at room temperature. Images were recorded during 60 s, and measurements obtained in a stable state (i.e., 30 s) are presented in this study. At least five measurements on each different surface were averaged to obtain reliable results.

For the CB contact angle, a homemade support for a quartz crystal sensor was created (Figure S1). Sensors were suspended face down,

Table 1. SAM Surface Properties

surface	chemical formula	SAM name	θ_{SD} pH 5 (deg)	θ_{CB} pH 5 (deg)	features	pK_a	charge at pH 5	$d_{MP\text{-}SPR}$ (nm)
CH_3	$HS(CH_2)_{17}CH_3$	UDT	104 ± 2	101 ± 1	hydrophobic		neutral	1.50 ± 0.31
NH_2	$HS(CH_2)_{11}NH_2 \cdot HCl$	AUT	67 ± 4	58 ± 2	hydrophilic	6.5	+	3.15 ± 0.74
COOH	$HS(CH_2)_{10}COOH$	MUA	22 ± 1	25 ± 2	hydrophilic	4.6	−	1.69 ± 0.27
OH	$HS(CH_2)_{11}OH$	MUD	26 ± 4	20 ± 3	hydrophilic		neutral	1.67 ± 0.66
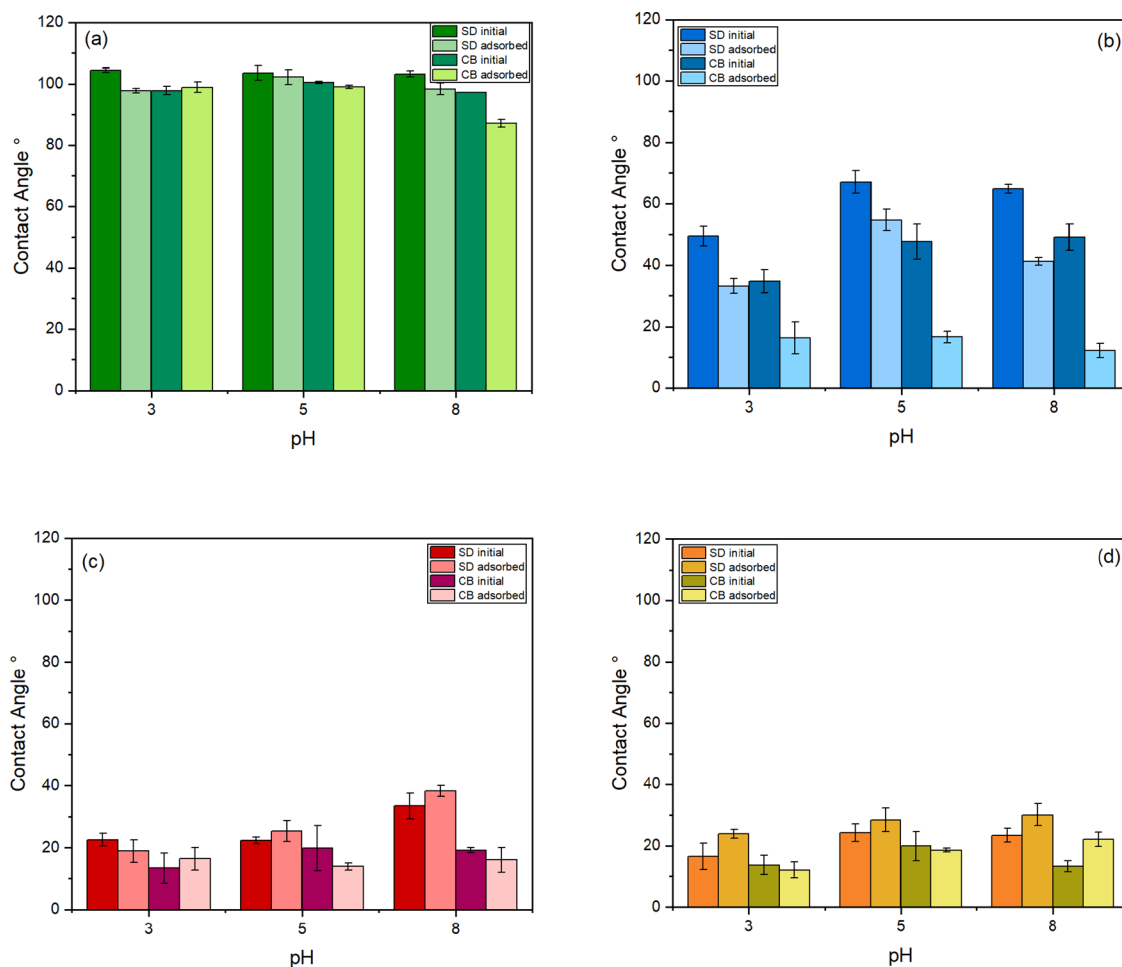
Figure 1. Contact angle measurements on SD and CB methods before and after *A. senegal* gum adsorption as a function of pH on (a) CH_3, (b) NH_2, (c) COOH, and (d) OH SAM functions.

and the support was submerged in a quartz tank, containing the buffer solution, by around 1 cm above the sensor. An air bubble with a volume of 5 μL was deposited at the interface by using a curved needle. To evaluate the surface pK_a of charged SAMs, i.e., MUA: −COOH and AUT: −NH$_2$, a CB experiment was used by varying the pH of the tank solution (50 mM NaCl degassed with N$_2$) over the same SAM surfaces. Experiments were carried out on two different sensors for both SAM surfaces.

The contact angles of all SAM surfaces, in both contact angle methods, were characterized immediately after functionalization, to control the SAM formation before adsorption, and right after gum adsorption in QCM-D to evaluate the impact of the gum on wettability. Sensors were kept in a buffer solution after the adsorption experiment and directly analyzed with CB contact angle measurement. After analysis, sensors were dried with N$_2$ for static contact angle measurement. While the SD contact angle can be directly measured (θ_{SD}), the CB contact angle must be recalculated since the angle measured is the contact angle between the air bubble and the solid surface with the following equation:[32]

$$\theta_{CB} = 180° - \theta_{air} \tag{3}$$

RESULTS AND DISCUSSION

Characterization of SAMs. SAM formations were characterized by contact angle measurements, and their thicknesses were measured by MP-SPR and ellipsometry. The obtained contact angles of SAM surfaces (Table 1) are consistent with the literature data.[16,20−23] Images of contact angle measurements at pH 5 in both methods are available in Table S2. As expected, the SD contact angle measurements suggested the most hydrophobic surface is −CH$_3$ (104° ± 2°), while the surfaces coated with the other groups are more polar: with −OH: 26° ± 4°; with − NH$_2$: 67° ± 4°; and with −COOH: 22° ± 1°. One hydrophobic interface (CH$_3$) and three more or less hydrophilic ones (OH, COOH) were therefore obtained. CB contact angle presents very similar results, with however a global tendency for the SAM surfaces to be more wettable when directly put in solution.

The apparent surface pK_a of SAMs has been investigated by different surface analysis techniques, such as quartz crystal microbalance,[33,34] surface plasmon resonance spectroscopy,[35]

C

chemical force microscopy,[36−38] indirect laser-induced temperature jump,[39] voltammetry,[40−42] and contact angle titration.[43] As shown by Marmisollé et al.,[41] the SAM apparent surface pK_a values vary depending on the chain length and the alkanethiol conformations, leading to some discrepancies in literature data. The apparent surface pK_a also varies according to ionic strength. In this study, the apparent surface pK_a of the two charged −COOH and −NH₂ SAMs was estimated through CB contact angle methods with 50 mM NaCl. This technique allows the complete wetting of the surface and thus the direct determination of the angle variation as a function of pH. CB measurement indicates that the SAM surface used in this study presents apparent pK_a at 4.6 and 6.5 for −COOH and −NH₂ SAMs, respectively (Figure S2).

The thicknesses of the SAMs were measured by MP-SPR in both air and buffer media before the gum adsorption (Table 1). SAM thicknesses were around 1.70 nm at the three studied pHs for all groups except for NH₂, where the thickness was double. The values are in agreement with previous studies.[20−23,44,45] The difference in NH₂ SAM thickness is probably due to steric constraints induced by hydrogen atoms overlapping. The SAM thicknesses were also measured by ellipsometry, right after the SAM formation, for comparison, and the present similar results were compared to those obtained using MP-SPR. The ellipsometry and MP-SPR results are presented in the Supporting Information (Table S3). SAM layer thicknesses are therefore identical before and after hydration in the buffer.

Monolayer formation depends on many factors such as adsorption time, temperature, the purity of the thiols, the quality of the Au surface, and also its roughness.[46,47] Discrepancy in contact angle or thicknesses between identical samples can indicate that the yield of SAMs is incomplete, and it presents defects or molecular disorders resulting in a discontinuous monolayer. Moreover, SAMs are sensitive to ultraviolet and thus can be unstable over time.[48] To prevent these drawbacks, SAM formation was controlled with contact angle measurements before each adsorption with only freshly prepared surfaces, and the impact of gum adsorption on those surfaces' contact angle was investigated right after the end of each experiment. These results will be discussed later.

Contact Angle Results. Surface contact angle measurements were performed on each QCM-D quartz before and after *A. senegal* adsorption (Figure 1), on both SD and CB methods to measure the gum adsorption impact on surface wettability in air and when immersed in a buffer. The CB method measures the wetting contact angle using an air bubble at a solid−liquid interface. This method is well suited for hydrophilic surfaces on which a liquid usually spreads out, making the SD method more difficult, and is more suitable to measure the wettability of surfaces that operate under a liquid.[32,49,50]

For all SAM surfaces, the total immersion in water leads to a slight increase of surface wettability, as discussed in the surface characterization section. From a general point of view, the contact angle variation after *A. senegal* gum adsorption is weak (<10°) except on the positively charged surface (−NH₂), where the impact on surface hydration is more visible. The following analysis mainly presents tendencies rather than quantitative issues.

A. senegal gum adsorption on the −CH₃ hydrophobic surface (Figure 1a) presents a weak influence on surface hydrophobicity, with only a little decrease of the contact angle,

particularly with the SD method. Despite the fact that angle variation is very weak for the −OH hydrophilic surface (Figure 1d), a small change is observed in the wettability of surfaces when the gum is adsorbed, particularly at pH 8, with this variation coming from the dehydration of the hydration shell rather than as a direct consequence of gum adsorption. Moreover, the wettability variation seems to be more visible at basic pH for −CH₃ and −OH SAMs on the CB method due to the less compact gum structure.[15,51]

On charged −NH₂ and −COOH surfaces, the gum adsorption affects the wettability differently according to the nature of the surface. The adsorption on the −NH₂ surface (Figure 1b) presents the highest impact on surface wettability, with a clear decrease of the contact angle in both methods when the gum is adsorbed. Interestingly, the variation of wettability could be related to the increase of the water content inside the layer structure. On the −COOH surface (Figure 1c), the impact of the adsorbed gum on surface wettability presents an opposite behavior depending on the contact method used. While the SD method shows an increase of the contact angle, the reverse is observed with the CB method. This wettability variation seems to follow surface pK_a. At low pH, the wettability decreases with gum adsorption, while at pH 5.0 and 8.0, the wettability increases. The reverse is observed when the surface is dried. Therefore, on a charged surface, the nature of the SAM function has an impact on gum-layer wettability.

Overall, when differences are significant, initially, more hydrophobic surfaces (CH₃, NH₂) result in a more polar final solid−gum interface, while more hydrophilic solid surfaces (OH, COOH) result in a less polar final interface. This is more obvious at pH 8 and illustrates experimentally the well-known dual hydrophilic/hydrophobic nature of *Acacia* gum.[26]

MP-SPR. The calculated adsorbed amount (Γ_{MP-SPR}) of *A. senegal* gum onto SAM surfaces as a function of pH obtained with MP-SPR experiments is presented in Figure 2. MP-SPR measures the "dry" adsorbed mass of the adsorbed molecules and is complementary to the QCM-D method. From a general point of view, the dry amount of *A. senegal* gum decreased as
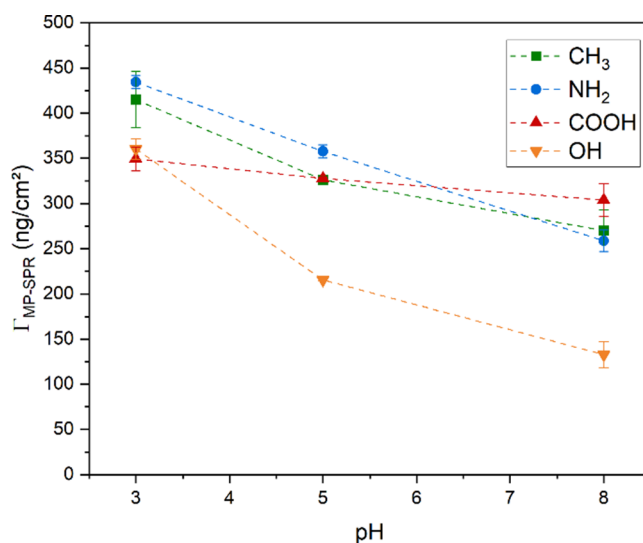
Figure 2. Equilibrium adsorbed amount (Γ_{MP-SPR}) of *A. senegal* gum onto SAM surfaces as a function of pH for CH₃ (green square), OH (orange inverted triangle), NH₂ (blue circle), and COOH (red upright triangle) SAM functions. *Lines are here to guide the eyes.*
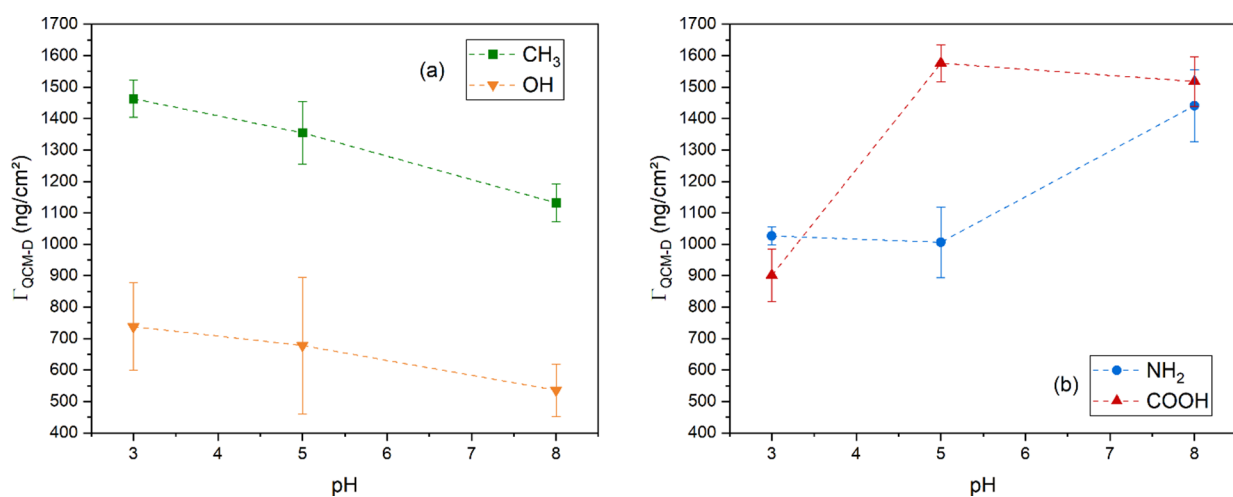
Figure 3. Equilibrium adsorbed amount ($\Gamma_{QCM\text{-}D}$) of *A. senegal* gum onto SAM surfaces as a function of pH for (a) CH$_3$ (green square) and OH (orange inverted triangle); or (b) NH$_2$ (blue circle) and COOH (red upright triangle) SAM functions. *Lines are here to guide the eyes.*

the pH increased for all surfaces. The interfacial concentration of gum is only significantly different near OH surfaces, except at pH 3, where surfaces containing the O atom were different from CH$_3$ and NH$_2$ surfaces. The adsorption on the −COOH function is very stable, with only a decrease of 13% between pH 3.0 and 8.0, while −CH$_3$ and −NH$_2$ surfaces present a more important impact of pH with 35−40% mass decrease at pH 8.0 (Figure 2). The purely hydrophilic surface presents the lowest adsorption and the highest pH influence with a decrease of 40% between pH 3 and 5, which reaches a 63% mass decrease at pH 8. According to Vogler,[52] the diffusion and adsorption of proteins to surfaces are strongly related to interphase dehydration. Moreover, the adsorbent capacity decreases with increasing hydrophilicity of the surfaces.[52] Therefore, *A. senegal* gum behaves at the interphase like proteins with the highest adsorbed dry amount on the hydrophobic surface at the three studied pHs. Surprisingly, the adsorbed *A. senegal* dry amounts on NH$_2$ and COOH SAMs, both hydrophilic and charged surfaces, were in the same order as the hydrophobic CH$_3$ one. This behavior might be due to the chemical properties of the *A. senegal* gum that contains both positive (amine group of amino acids) and negative (carboxyl group of amino acids and monosaccharides) charges. Consequently, the adsorption of *A. senegal* gum is mainly based on its hydrophobic and charge properties, allowing interphase dehydration, as previously discussed.[13]

Gum stability was also investigated with a desorption experiment (Figure S3). Gum adsorption is very stable, with less than 5% mass variation, except for the hydrophilic surface at pH 8.0, which reaches 10% mass loss. In line with our previous observations, the lesser the gum adsorbed, the less stable the adsorption.[10]

QCM-D. Adsorption of *A. senegal* gum on SAM surfaces as a function of pH was followed with the QCM-D technique, and the calculated mass adsorbed ($\Gamma_{QCM\text{-}D}$) is presented in Figure 3. Frequency change, related dissipation energy loss, shear elastic modulus, and shear viscosity are reported in Figures S4−S6.

Figure 3a presents the pH influence of gum adsorption on hydrophobic and hydrophilic surfaces (−CH$_3$ and −OH). The gum adsorption on hydrophobic and hydrophilic surfaces presents the same behavior over the pH range, with the decrease of the adsorbed mass with the increase of pH, as also

observed in MP-SPR. However, adsorption on the hydrophobic surface is double that on the hydrophilic surface. As in MP-SPR, the hydrophilic surface presents the lowest gum adsorption. The adsorption on CH$_3$−SAM was found to be maximal for many protein and polymeric systems.[53−57] As shown recently and previously discussed in the MP-SPR section, it is easier to dehydrate a hydrophobic interface (high surface tension) than an interface containing OH groups (low surface tension), explaining the highest interfacial gum concentration.[14] Indeed, the energetic cost of dehydrating a surface rises sharply with its hydrophilicity behavior.[52] Protein adsorption onto solid surfaces, whatever the amino acid composition, would therefore be controlled by water.[58] Figure 3b presents the pH impact of gum adsorption on charged surfaces (−COOH and −NH$_2$). The results show a clear impact of the surface charge over the "wet" gum adsorbed mass with an opposite behavior according to the charge nature. Indeed, a significant increase (75%) in the "wet" *A. senegal* amount adsorbed to the carboxylic surface was observed at pH 5.0 and 8.0, above the − COOH pK_a value of 4.6, when the chemical group was deprotonated and negatively charged. This behavior is in perfect agreement with previous studies performed on gold, TiO$_2$, SiO$_2$, and latex surfaces on which the "wet" adsorbed *A. senegal* mass increased as surfaces became negatively charged.[10−13,15] The negatively charged surfaces favor the "wet" protein moiety adsorption of the *A. senegal* gum due to attractive interactions between the negative surface and the positive charges of the protein moieties.[59] On the positively charged amine surface, an opposite effect was observed according to the charge surface with an increase of the "wet" adsorbed *A. senegal* mass as the charge surface was removed, above pK_a (Table 1). The effect of the positive charge on the surface may be related to a change of orientation of water molecules at the surface, as demonstrated by Moll et al.[60]

The present study therefore shows the direct impact of hydrophobicity/hydrophilicity and charge variations on the adsorption behavior of *A. senegal* gum. On an uncharged surface, the "wet" gum adsorption is maximum at acidic pH on both hydrophilic and hydrophobic surfaces. On charged surfaces, the adsorption of "wet" *A. senegal* gum behavior appeared antagonistic according to the charge sign of the surface: a negative charge favored "wet" gum adsorption, while

a positive one reduced it. As MP-SPR experiments showed a constant decrease with pH of "dry" *A. senegal* gum mass, QCM results certainly highlight differences in the hydration properties of the films (corresponding to SAM surface, interphase, and *A. senegal* gum) according to the polarity and charge of the surfaces that are discussed below (Figure 4).

Figure 4 presents the Γ_{QCM-D} value of *A. senegal* gum onto SAM surfaces as a function of the SD contact angle of SAM surfaces for the three pH conditions. At pH 3.0, the adsorption seems to follow the hydrophobicity of the surface. Indeed, at this pH, the −COOH surface should be uncharged, and therefore, only the surface hydrophobicity affects the gum adsorption, while the positive charge has no specific influence.

At pH 5.0 (Figure 4b), the addition of the negative charge has a clear impact on gum adsorption, and the adsorption no longer follows the hydrophobicity on the −COOH surfaces. By removing the unfavorable positive charge from the −NH₂ surface at pH 8.0 (Figure 4c), the wet gum adsorption largely increases, while the dry mass obtained using MP-SPR decreases. Hydration of the film should therefore increase at pH 8.0 (as discussed in the last paragraph of this study). In all experiments, the purely hydrophilic surface presents a lower adsorption capacity. Thus, a hydrophilic surface is unfavorable to *Acacia* gum adsorption, or to a difference of hydration, except if the surface presents a negative charge surface. Interestingly, the hydrophobic surface presents less adsorbed mass than the negatively charged surface. Thus, SAM surfaces show that Coulomb-type electrostatic interactions have an important effect on the *Acacia* gum "wet" mass adsorbed. Kékicheff[61] clearly demonstrated that the long-range attractive hydrophobic forces between macroscopic surfaces have an electrostatic origin. Other authors rationalized the adsorption onto solid surfaces by a correlation between independent electrostatic and hydration forces.[62]

Dynamic changes in the layer conformation or the hydration water content during the gum adsorption experiment can be analyzed by plotting the D−f plots from the QCM-D experiments (ΔD vs ΔF curves)[25,63,64] as presented in Figure 5. The viscoelastic properties of the layer are related to the curve slope, also called regime (|ΔD/ΔF|). A viscoelastic and hydrated layer will present a higher |ΔD/ΔF| value than a more elastic and less hydrated layer, while a slope rupture is characteristic of a conformational change during the adsorption process.[13] It is now well-known that *Acacia* gum adsorption occurs through various conformational changes or rearrangements in time.[10,11,13] However, the gum-layer behavior varies according to the nature of the surface and the pH condition.

At least two different regimes can be observed for each curve. The first slope, or regime, corresponds to the initial state of the gum when it adsorbs on the SAM surface. Hydrophobic (UDT) and −COOH (MUA) surfaces present similar curves with two different behaviors depending on the pH. At acidic pH, layers present a slightly more rigid behavior with almost no dynamic changes. The increase in the pH increases the layer viscoelastic properties, in conjunction with an increase of both *Acacia* gum and film hydration, with a higher |ΔD/ΔF| value. It is therefore interesting to note that although the two surfaces are in opposite states of hydrophobicity, the viscoelastic properties of the gum layer behave in a similar way according to the D−f plot. The −NH₂ surface (AUT) presents the greatest pH impact on layer viscoelasticity. At pH 3.0, the −NH₂ surface is positively charged, and the gum film exhibits a
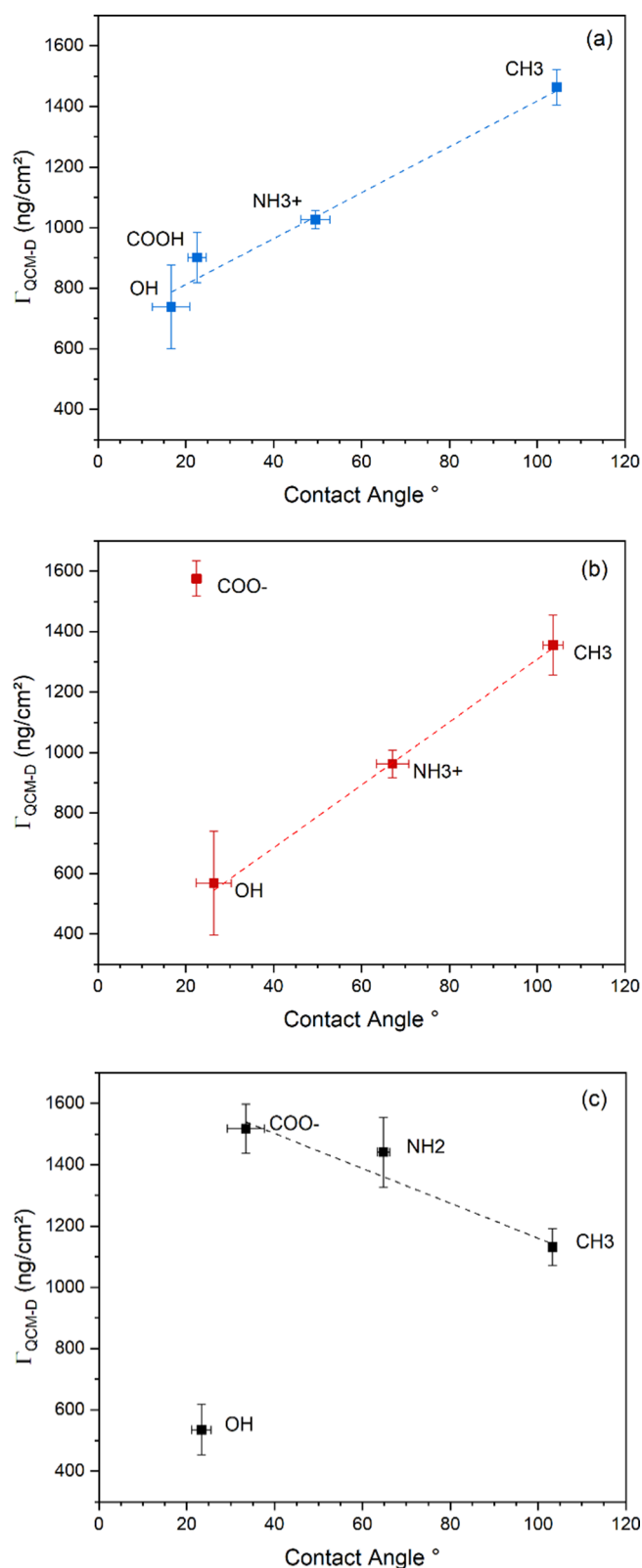
Figure 4. Adsorbed amount (Γ_{QCM-D}) of part *A. senegal* gum onto SAM surfaces in the equilibrium state as a function of the initial SAM surface SD contact angle at (a) pH 3.0, (b) pH 5.0, and (c) pH 8.0. *Lines are here to guide the eyes.*

more rigid behavior during the initial adsorption state, with a very low |ΔD/ΔF| value. This behavior was already observed on the TiO₂ surface.[13] Increasing the pH induces an increase in
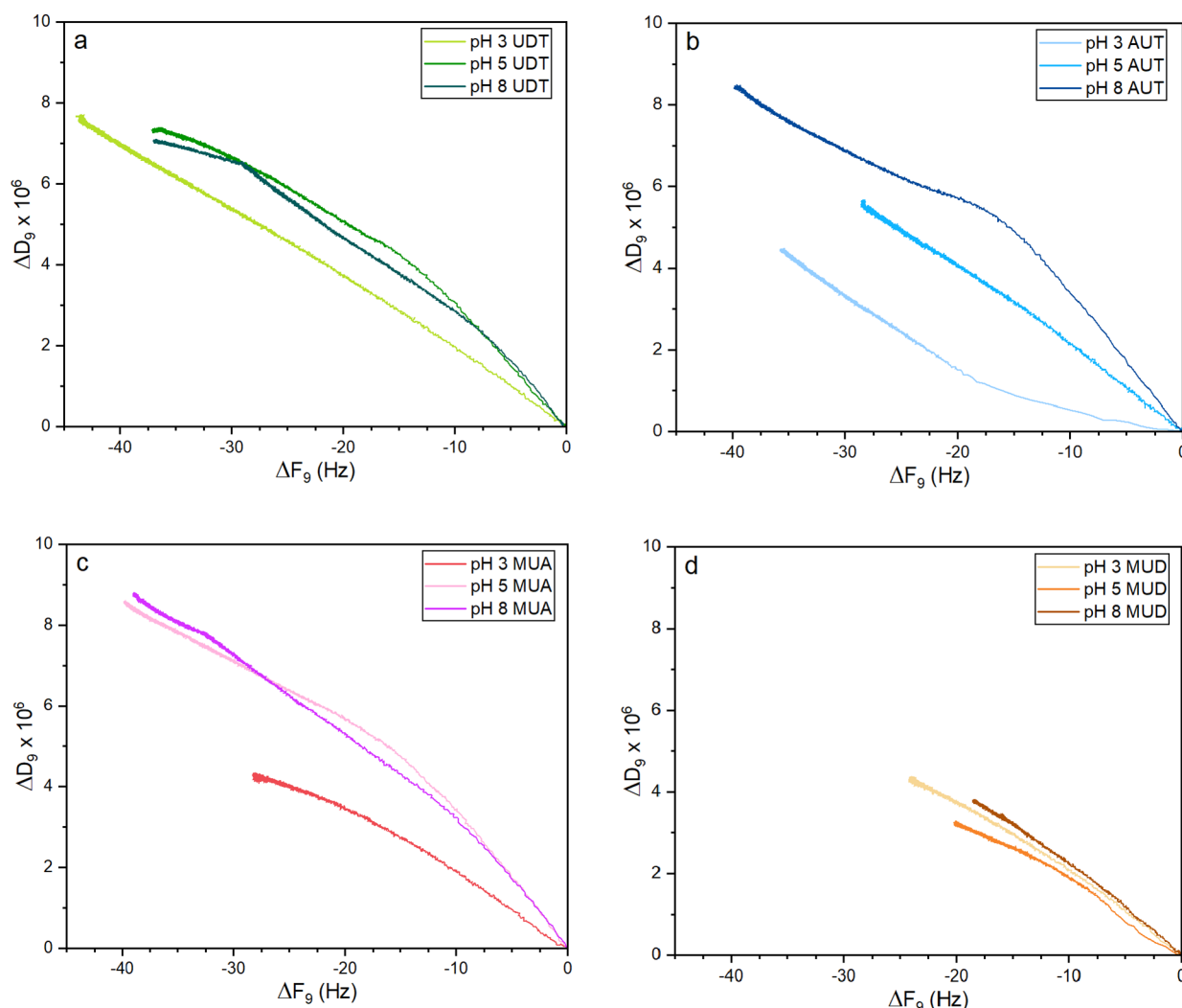
Figure 5. $D-f$ plots from the ninth overtone of part *A. senegal* as a function of pH during the adsorption process on SAM surfaces: (a) CH_3, (b) NH_2, (c) COOH, and (d) OH.

film viscoelasticity, resulting in three different viscoelastic behaviors, i.e., three different initial $|\Delta D/\Delta F|$ values. However, compared to the oxide surface, there is no clear impact of the pH on viscoelastic properties of the gum film adsorbed on a hydrophilic surface (MUD), i.e., the three curves are superimposed with similar dynamic changes. Considering the dynamic change, a stiffening of layers generally occurs with conformational changes on SAM surfaces, i.e., the last slope presents a more rigid behavior than the first one with a lower $|\Delta D/\Delta F|$ value, indicating progressive interfacial dehydration of the gum structure. A similar behavior was reported in previous studies for *Acacia* gum[10,11,13] but also for protein on hydrophobic surfaces.[19,65,66] The only exception is for the positively charged surface at pH 3.0, which presents an increase in the viscoelastic properties with the conformational change, due to the gum capacity of adaptation through conformational change and dehydration to reach the steadiest and an efficient state on a solid surface.[13]

Desorption experiments (Figure S7) show that all adsorbed SAM layers are very stable at pH 3.0 and 5.0. However, at pH 8.0, while −COOH and −NH_2 surfaces show no desorption or swelling modification, −CH_3 and −OH surfaces present an increase of the wet mass, corresponding to the slight swelling of the layers after adsorption (less than 5%). Considering that

the QCM-D technique records the "wet" mass of the adsorbed gum, which includes water in the hydration shells and "trapped" inside the gum layer, the hydration percentage of the adsorbed film (% H_2O) can be estimated (Figure 6) by combining the MP-SPR results (see the Materials and Methods section).

Generally, there is an increase in the % H_2O when the pH solution increases. However, the % H_2O variation varies according to the SAM surfaces. The hydrophobic surface layers present a high water content (72−76%) and are slightly affected by the pH variation. Surprisingly, there is a large variation of the water percentage layer on the hydrophilic surface, from 51 to 75% between acidic and basic pH conditions, while the viscoelastic properties were similar in the three pH conditions (cf. $D-f$ plots in Figure 5). Therefore, changes in hydration of layers on −OH surfaces apparently only involve water of hydration shells and/or on the SAM surface but not water molecules inside the layer structure. The −COOH SAM surface shows an increase of the water content from 61 to 79% after its pK_a due to the activation of the negative charge. Interestingly, the water contents of the adsorbed layer on hydrophobic and −COOH surfaces are quite similar, especially at pH 5.0 and 8.0. This observation confirms that −CH_3 and −COOH adsorbed layers present a
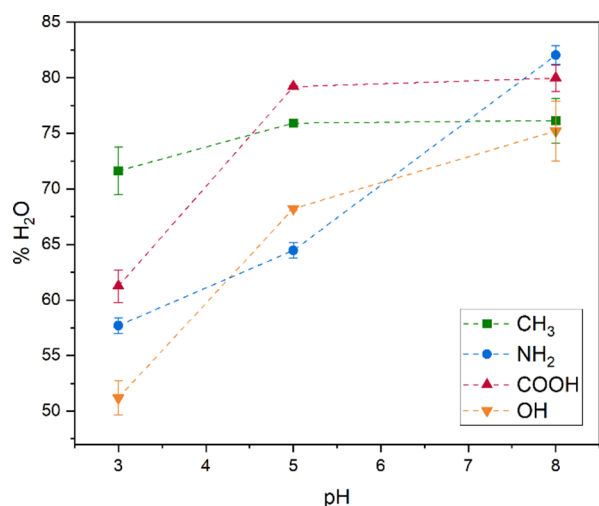
Figure 6. % H$_2$O of the part *A. senegal* gum layer onto SAM surfaces in the equilibrium state as a function of pH for CH$_3$ (green square), OH (orange inverted triangle), NH$_2$ (blue circle), and COOH (red upright triangle) SAM functions. *Lines are here to guide the eyes.*

similar structure and viscoelastic behavior. The positively charged surface presents a slightly more linear increase over the pH range studied, in agreement with the variation of the layers' viscoelastic behavior over the pH range. At pH 8.0, *A. senegal* gum layers are highly hydrated and present similar water content between 75 and 81% whatever the SAM surfaces. It was therefore recently demonstrated that *A. seyal* gum aggregates completely dissociated above pH 8, in agreement with the increase of hydration.[67] One hypothesis

would be that the excess of positive charges comes from histidine residues (∼6% w/w) that would be involved in the dissociation process. At high pH, acid groups present in *Acacia* gum (−COO$^-$) in both protein (10% of aspartic and glutamic acids) and carbohydrate (16% of glucuronic acids) become fully ionized, resulting in the "swelling" of the carbohydrate moieties and thus leading to a more hydrophilic and hydrated gum as observed by Ma et al.[51] However, at acidic pH, the gum becomes fully protonated and becomes less hydrophilic with the "compression" of its structure. The change of structure with pH was corroborated using small-angle X-ray scattering (Figure S6), where the normalized Kratky plots clearly show that *Acacia* gum is less globular and slightly unfolded at pH 5 and pH 8, giving rise to a "swelling" or expansion of the structure, while a more compact conformation is observed at pH 3. A greater variation in the layer swelling can thus be observed depending on the nature of the SAM surface, with the hydrophilic surface presenting the lowest water content (51%) and the hydrophobic surface presenting the highest water content (72%). These results are in agreement with our previous study,[15] which has demonstrated a more aggregated and less hydrogen-bonded adsorbed layer at acidic conditions, while a more hydrated adsorbed layer was observed after a change in the secondary structure of the protein moieties at a higher pH on gold nanoparticles.

Figure 7 summarizes the scientific context and the main results obtained in the present study, where a subtle interplay between surface hydration and gum dehydration plays a pivotal role in the adsorption properties.
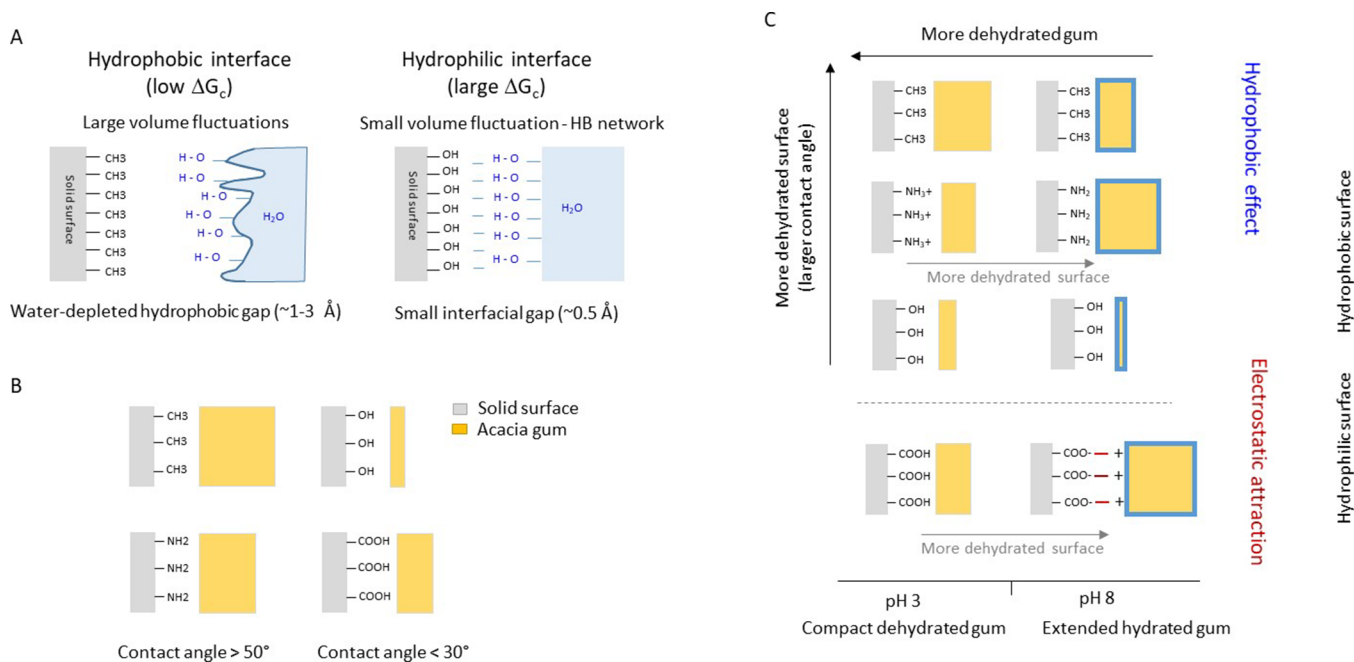
Figure 7. Schematic illustration of the scientific problem and the main results obtained. (A) Physical differences between a hydrophobic and a hydrophilic solid−water interface. For the hydrophobic case, uncoordinated water promotes a large contact angle and large interfacial volume fluctuations occur, which lowers the Gibbs free energy of cavity creation (DG$_c$) at the interface. This is favorable to the interface dehydration and the formation of a viscoelastic structure. For the hydrophilic case, hydrogen-bond (HB) interactions between the surface and water render dehydration more difficult, resulting in a less concentrated interface. (B) Effect of contact angle on the amount of gum at the solid−water interface. (C) Combined effect of interface hydrophobicity/hydrophilicity and gum hydration on the amount of gum at the solid−water interface at pH 3 and 8.

CONCLUSIONS

The use of QCM-D and MP-SPR techniques enables the investigation of the adsorption behavior of *Acacia senegal* gum on SAMs by varying the hydrophobicity and charge properties of the surfaces. This study demonstrates that despite the surface being hydrophilic, *A. senegal* gum will adsorb strongly if the surface contains negative charges. The adsorbed layer presents the highest dry mass but the lowest water content at pH 3.0 whatever the SAM surface, while the wet mass adsorbed follows surface hydrophobicity. The increase in pH leads to a reduction in the adsorbed dry mass and an increase in the hydration rate and viscoelastic properties of the layer for all SAM surfaces but with a different intensity depending on the surface property. The greatest variation is observed on a purely hydrophilic surface, whereas a hydrophobic surface is less affected and thus more stable over pH. The impact of the negative charge is significant in increasing the hydration rate of the adsorbed layer. However, a positive charge drastically affects the layer viscoelastic properties by forming a more rigid and less hydrated layer at a low pH.

The contact angle experiments have shown that the CB method is more suitable to measure the wettability variation of the surfaces before and after gum adsorption. On hydrophobic surfaces, the gum layer slightly increases the wettability, while on hydrophilic surfaces, the variation is less significant. Only the $-NH_2$ surface presents a significant wettability increase with the pH, indicating the formation of a more homogeneous layer compared to over the SAM surface.

This study aimed to explore the relative importance of the polarity of solid surfaces and biopolymers from *Acacia* gum on the extent of adsorption of the latter. Generally, enhanced water−surface or water−biopolymer interactions do not favor the interfacial concentration of the gum through impaired interfacial dehydration. However, while pH significantly influences the dry mass adsorption of the gum, it is the variation in surface properties, mainly surface charge and hydrophobicity, that has the greatest impact on adsorbed gum hydration and thus its viscoelastic properties.

ASSOCIATED CONTENT

ⓈI Supporting Information

The Supporting Information is available free of charge at https://pubs.acs.org/doi/10.1021/acs.langmuir.4c02002.

> Biochemical composition and structural parameter of *A. senegal* gum, CB contact angle information and measurement images, surface pK_a measurement, ellipsometry method details and results, frequency change and dissipation energy loss of QCM-D experiments, shear elastic modulus and shear viscosity calculated from QCM-D, SAXS curves of *A. senegal* as a function of pH, and desorption effect in QCM-D and MP-SPR (PDF)

AUTHOR INFORMATION

Corresponding Author

Denis Renard − *INRAE, UR BIA, F-44316 Nantes, France*; ⓞ orcid.org/0000-0001-9495-7660; Email: denis.renard@inrae.fr

Authors

Athénaïs Davantès − *INRAE, UR BIA, F-44316 Nantes, France*; ⓞ orcid.org/0000-0001-5376-4053

Michaël Nigen − *UMR IATE, Univ Montpellier, INRAE, Institut Agro, 34060 Montpellier, France*

Christian Sanchez − *UMR IATE, Univ Montpellier, INRAE, Institut Agro, 34060 Montpellier, France*

Complete contact information is available at:
https://pubs.acs.org/10.1021/acs.langmuir.4c02002

Author Contributions

A.D. contributed by designing, performing the experiments, analyzing the data, and writing the paper. M.N., C.S., and D.R. contributed by analyzing the data and writing the paper. All authors have given approval to the final version of the manuscript.

Notes

The authors declare no competing financial interest.

ACKNOWLEDGMENTS

ABBREVIATIONS

SD:sessile drop; CB:captive bubble; SAMs:self-assembled monolayers; QCM-D:quartz crystal microbalance with dissipation; MP-SPR:multiparametric surface plasmon resonance

REFERENCES

(1) Zhao, C.; Liu, G.; Tan, Q.; Gao, M.; Chen, G.; Huang, X.; Xu, X.; Li, L.; Wang, J.; Zhang, Y.; Xu, D. Polysaccharide-Based Biopolymer Hydrogels for Heavy Metal Detection and Adsorption. *J. Adv. Res.* **2023**, *44*, 53−70.

(2) Pandey, S.; Son, N.; Kim, S.; Balakrishnan, D.; Kang, M. Locust Bean Gum-Based Hydrogels Embedded Magnetic Iron Oxide Nanoparticles Nanocomposite: Advanced Materials for Environmental and Energy Applications. *Environ. Res.* **2022**, *214*, No. 114000.

(3) Tan, C.; Feng, B.; Zhang, X.; Xia, W.; Xia, S. Biopolymer-Coated Liposomes by Electrostatic Adsorption of Chitosan (Chitosomes) as Novel Delivery Systems for Carotenoids. *Food Hydrocoll.* **2016**, *52*, 774−784.

(4) Rahikainen, J. L.; Martin-Sampedro, R.; Heikkinen, H.; Rovio, S.; Marjamaa, K.; Tamminen, T.; Rojas, O. J.; Kruus, K. Inhibitory Effect of Lignin during Cellulose Bioconversion: The Effect of Lignin Chemistry on Non-Productive Enzyme Adsorption. *Bioresour. Technol.* **2013**, *133*, 270−278.

(5) Thipe, V. C.; Amiri, K. P.; Bloebaum, P.; Karikachery, A. R.; Khoobchandani, M.; Katti, K. K.; Jurisson, S. S.; Katti, K. V. Development of Resveratrol-Conjugated Gold Nanoparticles: Interrelationship of Increased Resveratrol Corona on Anti-Tumor Efficacy against Breast, Pancreatic and Prostate Cancers. *Int. J. Nanomed.* **2019**, *14*, 4413−4428.

(6) Makvandi, P.; Baghbantaraghdari, Z.; Zhou, W.; Zhang, Y.; Manchanda, R.; Agarwal, T.; Wu, A.; Maiti, T. K.; Varma, R. S.; Smith, B. R. Gum Polysaccharide/Nanometal Hybrid Biocomposites in Cancer Diagnosis and Therapy. *Biotechnol. Adv.* **2021**, *48*, No. 107711.

(7) Nussinovitch, A. *Plant Gum Exudates of the World: Sources, Distribution, Properties, and Applications*; CRC Press, 2009.

(8) Sanchez, C.; Nigen, M.; Mejia Tamayo, V.; Doco, T.; Williams, P.; Amine, C.; Renard, D. Acacia Gum: History of the Future. *Food Hydrocoll.* **2018**, *78*, 140−160.

(9) Renard, D.; Lavenant-Gourgeon, L.; Ralet, M.-C.; Sanchez, C. Acacia Senegal Gum: Continuum of Molecular Species Differing by Their Protein to Sugar Ratio, Molecular Weight, and Charges. *Biomacromolecules* **2006**, *7* (9), 2637−2649.

(10) Davantès, A.; Nigen, M.; Sanchez, C.; d'Orlando, A.; Renard, D. Adsorption of Hyperbranched Arabinogalactan-Proteins from Plant Exudate at the Solid−Liquid Interface. *Colloids Interfaces* **2019**, *3* (2), 49.

(11) Davantès, A.; Nigen, M.; Sanchez, C.; Renard, D. Adsorption Behavior of Arabinogalactan-Proteins (AGPs) from Acacia Senegal Gum at a Solid−Liquid Interface. *Langmuir* **2021**, *37* (35), 10547−10559.

(12) Renard, D.; Davantès, A.; D'orlando, A.; Cahier, K.; Molinari, M.; Nigen, M.; Chalier, P.; Sanchez, C. Adsorption of Arabinoga-lactan-Proteins from Acacia Gums (Senegal and Seyal) and Its Molecular Fractions onto Latex Particles. *Food Hydrocoll.* **2022**, *125*, No. 107360.

(13) Davantès, A.; Nigen, M.; Sanchez, C.; Renard, D. Impact of Hydrophobic and Electrostatic Forces on the Adsorption of Acacia Gum on Oxide Surfaces Revealed by QCM-D. *Colloids Interfaces* **2023**, *7* (2), 26.

(14) Faucon, C.; Chalier, P.; Sanchez, C. Natural Hyperbranched Biopolymer at Liquid Interfaces Differing in Oil−Water Interaction Energy. *J. Mol. Liq.* **2023**, *384*, No. 122175.

(15) Davantès, A.; Nigen, M.; Sanchez, C.; Renard, D. *In Situ* ATR Spectroscopy Study of the Interaction of *Acacia Senegal* Gum with Gold Nanoparticles Films at the Solid−Liquid Interface. *Langmuir* **2024**, *40* (1), 529−540.

(16) Attwood, S. J.; Kershaw, R.; Uddin, S.; Bishop, S. M.; Welland, M. E. Understanding How Charge and Hydrophobicity Influence Globular Protein Adsorption to alkanethiol and Material Surfaces. *J. Mater. Chem. B* **2019**, *7* (14), 2349−2361.

(17) Lebec, V.; Landoulsi, J.; Boujday, S.; Poleunis, C.; Pradier, C.-M.; Delcorte, A. Probing the Orientation of β-Lactoglobulin on Gold Surfaces Modified by Alkyl Thiol Self-Assembled Monolayers. *J. Phys. Chem. C* **2013**, *117* (22), 11569−11577.

(18) Hajiraissi, R.; Hanke, M.; Yang, Y.; Duderija, B.; Gonzalez Orive, A.; Grundmeier, G.; Keller, A. Adsorption and Fibrillization of Islet Amyloid Polypeptide at Self-Assembled Monolayers Studied by QCM-D, AFM, and PM-IRRAS. *Langmuir* **2018**, *34* (11), 3517−3524.

(19) Anand, G.; Sharma, S.; Dutta, A. K.; Kumar, S. K.; Belfort, G. Conformational Transitions of Adsorbed Proteins on Surfaces of Varying Polarity. *Langmuir* **2010**, *26* (13), 10803−10811.

(20) Phan, H. T. M.; Bartelt-Hunt, S.; Rodenhausen, K. B.; Schubert, M.; Bartz, J. C. Investigation of Bovine Serum Albumin (BSA) Attachment onto Self-Assembled Monolayers (SAMs) Using Combinatorial Quartz Crystal Microbalance with Dissipation (QCM-D) and Spectroscopic Ellipsometry (SE). *PLoS One* **2015**, *10* (10), No. e0141282.

(21) Kazzaz, A. E.; Fatehi, P. Interaction of Synthetic and Lignin-Based Sulfonated Polymers with Hydrophilic, Hydrophobic, and Charged Self-Assembled Monolayers. *RSC Adv.* **2020**, *10* (60), 36778−36793.

(22) Pranzetti, A.; Salaün, S.; Mieszkin, S.; Callow, M. E.; Callow, J. A.; Preece, J. A.; Mendes, P. M. Model Organic Surfaces to Probe Marine Bacterial Adhesion Kinetics by Surface Plasmon Resonance. *Adv. Funct. Mater.* **2012**, *22* (17), 3672−3681.

(23) Contreras, A. E.; Steiner, Z.; Miao, J.; Kasher, R.; Li, Q. Studying the Role of Common Membrane Surface Functionalities on Adsorption and Cleaning of Organic Foulants Using QCM-D. *Environ. Sci. Technol.* **2011**, *45* (15), 6309−6315.

(24) Choi, J.-H.; Kim, S.-O.; Linardy, E.; Dreaden, E. C.; Zhdanov, V. P.; Hammond, P. T.; Cho, N.-J. Adsorption of Hyaluronic Acid on Solid Supports: Role of pH and Surface Chemistry in Thin Film Self-Assembly. *J. Colloid Interface Sci.* **2015**, *448*, 197−207.

(25) Sedeva, I. G.; Fornasiero, D.; Ralston, J.; Beattie, D. A. Reduction of Surface Hydrophobicity Using a Stimulus-Responsive Polysaccharide. *Langmuir* **2010**, *26* (20), 15865−15874.

(26) Mejia Tamayo, V.; Nigen, M.; Apolinar-Valiente, R.; Doco, T.; Williams, P.; Renard, D.; Sanchez, C. Flexibility and Hydration of Amphiphilic Hyperbranched Arabinogalactan-Protein from Plant Exudate: A Volumetric Perspective. *Colloids Interfaces* **2018**, *2* (1), 11.

(27) Höök, F.; Rodahl, M.; Brzezinski, P.; Kasemo, B. Energy Dissipation Kinetics for Protein and Antibody−Antigen Adsorption under Shear Oscillation on a Quartz Crystal Microbalance. *Langmuir* **1998**, *14* (4), 729−734.

(28) Rodahl, M.; Höök, F.; Krozer, A.; Brzezinski, P.; Kasemo, B. Quartz Crystal Microbalance Setup for Frequency and Q-factor Measurements in Gaseous and Liquid Environments. *Rev. Sci. Instrum.* **1995**, *66* (7), 3924−3930.

(29) Voinova, M. V.; Rodahl, M.; Jonson, M.; Kasemo, B. Viscoelastic Acoustic Response of Layered Polymer Films at Fluid-Solid Interfaces: Continuum Mechanics Approach. *Phys. Scr.* **1999**, *59* (5), 391.

(30) Höök, F.; Kasemo, B.; Nylander, T.; Fant, C.; Sott, K.; Elwing, H. Variations in Coupled Water, Viscoelastic Properties, and Film Thickness of a Mefp-1 Protein Film during Adsorption and Cross-Linking: A Quartz Crystal Microbalance with Dissipation Monitoring, Ellipsometry, and Surface Plasmon Resonance Study. *Anal. Chem.* **2001**, *73* (24), 5796−5804.

(31) Reviakine, I.; Johannsmann, D.; Richter, R. P. Hearing What You Cannot See and Visualizing What You Hear: Interpreting Quartz Crystal Microbalance Data from Solvated Interfaces. *Anal. Chem.* **2011**, *83* (23), 8838−8848.

(32) Prydatko, A. V.; Belyaeva, L. A.; Jiang, L.; Lima, L. M. C.; Schneider, G. F. Contact Angle Measurement of Free-Standing Square-Millimeter Single-Layer Graphene. *Nat. Commun.* **2018**, *9* (1), 4185.

(33) Sugihara, K.; Teranishi, T.; Shimazu, K.; Uosaki, K. Structure Dependence of the Surface pKa of Mercaptoundecanoic Acid SAM on Gold. *Electrochemistry* **1999**, *67* (12), 1172−1174.

(34) Shimazu, K.; Teranishi, T.; Sugihara, K.; Uosaki, K. Surface Mass Titrations of Self-Assembled Monolayers of ω-Mercaptoalka-noic Acids on Gold. *Chem. Lett.* **1998**, *27* (7), 669−670.

(35) Fears, K. P.; Creager, S. E.; Latour, R. A. Determination of the Surface pK of Carboxylic- and Amine-Terminated Alkanethiols Using Surface Plasmon Resonance Spectroscopy. *Langmuir* **2008**, *24* (3), 837−843.

(36) Noy, A.; Vezenov, D. V.; Lieber, C. M. Chemical Force Microscopy. *Annu. Rev. Mater. Sci.* **1997**, *27* (1), 381−421.

(37) Wallwork, M. L.; Smith, D. A.; Zhang, J.; Kirkham, J.; Robinson, C. Complex Chemical Force Titration Behavior of Amine-Terminated Self-Assembled Monolayers. *Langmuir* **2001**, *17* (4), 1126−1131.

(38) Zhang, H.; He, H.-X.; Wang, J.; Mu, T.; Liu, Z.-F. Force Titration of Amino Group-Terminated Self-Assembled Monolayers Using Chemical Force Microscopy. *Appl. Phys. A: Mater. Sci. Process.* **1998**, *66* (1), S269−S271.

(39) Smalley, J. F.; Chalfant, K.; Feldberg, S. W.; Nahir, T. M.; Bowden, E. F. An Indirect Laser-Induced Temperature Jump Determination of the Surface pKa of 11-Mercaptoundecanoic Acid Monolayers Self-Assembled on Gold. *J. Phys. Chem. B* **1999**, *103* (10), 1676−1685.

(40) Munakata, H.; Oyamatsu, D.; Kuwabata, S. Effects of ω-Functional Groups on pH-Dependent Reductive Desorption of alkanethiol Self-Assembled Monolayers. *Langmuir* **2004**, *20* (23), 10123−10128.

(41) Marmisollé, W. A.; Capdevila, D. A.; de la Llave, E.; Williams, F. J.; Murgida, D. H. Self-Assembled Monolayers of NH2-Terminated Thiolates: Order, pKa, and Specific Adsorption. *Langmuir* **2013**, *29* (17), 5351−5359.

(42) Degefa, T. H.; Schön, P.; Bongard, D.; Walder, L. Elucidation of the Electron Transfer Mechanism of Marker Ions at SAMs with Charged Head Groups. *J. Electroanal. Chem.* **2004**, *574* (1), 49−62.

(43) Creager, S. E.; Clarke, J. Contact-Angle Titrations of Mixed.Omega.-Mercaptoalkanoic Acid/alkanethiol Monolayers on Gold. Reactive vs Nonreactive Spreading, and Chain Length Effects on Surface pKa Values. *Langmuir* **1994**, *10* (10), 3675−3683.

(44) Damos, F. S.; Luz, R. C. S.; Kubota, L. T. Determination of Thickness, Dielectric Constant of Thiol Films, and Kinetics of Adsorption Using Surface Plasmon Resonance. *Langmuir* **2005**, *21* (2), 602−609.

(45) Szefczyk, B.; Franco, R.; Gomes, J. A. N. F.; Cordeiro, M. N. D. S. Structure of the Interface between Water and Self-Assembled Monolayers of Neutral, Anionic and Cationic Alkane Thiols. *J. Mol. Struct. THEOCHEM* **2010**, *946* (1−3), 83−87.

(46) Love, J. C.; Estroff, L. A.; Kriebel, J. K.; Nuzzo, R. G.; Whitesides, G. M. Self-Assembled Monolayers of Thiolates on Metals as a Form of Nanotechnology. *Chem. Rev.* **2005**, *105* (4), 1103−1170.

(47) Vericat, C.; Vela, M. E.; Benitez, G.; Carro, P.; Salvarezza, R. C. Self-Assembled Monolayers of Thiols and Dithiols on Gold: New Challenges for a Well-Known System. *Chem. Soc. Rev.* **2010**, *39* (5), 1805−1834.

(48) Evans, S. D.; Sharma, R.; Ulman, A. Contact Angle Stability: Reorganization of Monolayer Surfaces? *Langmuir* **1991**, *7* (1), 156−161.

(49) Moraila, C. L.; Montes Ruiz-Cabello, F. J.; Cabrerizo-Vílchez, M.; Rodríguez-Valverde, M. Á. Wetting Transitions on Rough Surfaces Revealed with Captive Bubble Experiments. The Role of Surface Energy. *J. Colloid Interface Sci.* **2019**, *539*, 448−456.

(50) Dorrer, C.; Rühe, J. Superaerophobicity: Repellence of Air Bubbles from Submerged, Surface-Engineered Silicon Substrates. *Langmuir* **2012**, *28* (42), 14968−14973.

(51) Ma, F.; Bell, A. E.; Davis, F. J. Effects of High-Hydrostatic Pressure and pH Treatments on the Emulsification Properties of Gum Arabic. *Food Chem.* **2015**, *184*, 114−121.

(52) Vogler, E. A. Protein Adsorption in Three Dimensions. *Biomaterials* **2012**, *33* (5), 1201−1237.

(53) Zhang, P.; Chen, Y.-P.; Guo, J.-S.; Shen, Y.; Yang, J.-X.; Fang, F.; Li, C.; Gao, X.; Wang, G.-X. Adsorption Behavior of Tightly Bound Extracellular Polymeric Substances on Model Organic Surfaces under Different pH and Cations with Surface Plasmon Resonance. *Water Res.* **2014**, *57*, 31−39.

(54) Silin, V.; Weetall, H.; Vanderah, D. J. SPR Studies of the Nonspecific Adsorption Kinetics of Human IgG and BSA on Gold Surfaces Modified by Self-Assembled Monolayers (SAMs). *J. Colloid Interface Sci.* **1997**, *185* (1), 94−103.

(55) Peng, C.; Liu, J.; Zhao, D.; Zhou, J. Adsorption of Hydrophobin on Different Self-Assembled Monolayers: The Role of the Hydrophobic Dipole and the Electric Dipole. *Langmuir* **2014**, *30* (38), 11401−11411.

(56) Martins, M. C. L.; Fonseca, C.; Barbosa, M. A.; Ratner, B. D. Albumin Adsorption on Alkanethiols Self-Assembled Monolayers on Gold Electrodes Studied by Chronopotentiometry. *Biomaterials* **2003**, *24* (21), 3697−3706.

(57) Cha, P.; Krishnan, A.; Fiore, V. F.; Vogler, E. A. Interfacial Energetics of Protein Adsorption from Aqueous Buffer to Surfaces with Varying Hydrophilicity. *Langmuir* **2008**, *24* (6), 2553−2563.

(58) Faucon, C.; Chalier, P.; Sanchez, C. On the Relationship between Volume Fluctuations in Liquids and the Gibbs Free Energy of Cavity Formation. *J. Mol. Liq.* **2022**, *364*, No. 119845.

(59) Wasilewska, M.; Adamczyk, Z. Fibrinogen Adsorption on Mica Studied by AFM and in Situ Streaming Potential Measurements. *Langmuir* **2011**, *27* (2), 686−696.

(60) Moll, C. J.; Versluis, J.; Bakker, H. J. Direct Evidence for a Surface and Bulk Specific Response in the Sum-Frequency Generation Spectrum of the Water Bend Vibration. *Phys. Rev. Lett.* **2021**, *127* (11), No. 116001.

(61) Kékicheff, P. The Long-Range Attraction between Hydrophobic Macroscopic Surfaces. *Adv. Colloid Interface Sci.* **2019**, *270*, 191−215.

(62) Klaassen, A.; Liu, F.; Mugele, F.; Siretanu, I. Correlation between Electrostatic and Hydration Forces on Silica and Gibbsite Surfaces: An Atomic Force Microscopy Study. *Langmuir* **2022**, *38* (3), 914−926.

(63) Höök, F.; Rodahl, M.; Kasemo, B.; Brzezinski, P. Structural Changes in Hemoglobin during Adsorption to Solid Surfaces: Effects of pH, Ionic Strength, and Ligand Binding. *Proc. Natl. Acad. Sci. U. S. A.* **1998**, *95* (21), 12271−12276.

(64) Guo, S.; Pranantyo, D.; Kang, E.-T.; Loh, X. J.; Zhu, X.; Jańczewski, D.; Neoh, K. G. Dominant Albumin−Surface Interactions under Independent Control of Surface Charge and Wettability. *Langmuir* **2018**, *34* (5), 1953−1966.

(65) Molino, P. J.; Higgins, M. J.; Innis, P. C.; Kapsa, R. M. I.; Wallace, G. G. Fibronectin and Bovine Serum Albumin Adsorption and Conformational Dynamics on Inherently Conducting Polymers: A QCM-D Study. *Langmuir* **2012**, *28* (22), 8433−8445.

(66) Jia, P.; He, M.; Gong, Y.; Chu, X.; Yang, J.; Zhao, J. Probing the Adjustments of Macromolecules during Their Surface Adsorption. *ACS Appl. Mater. Interfaces* **2015**, *7* (12), 6422−6429.

(67) Antoine-Michard, A. *Agrégation Des Arabinogalactane-Protéines de La Gomme d'Acacia Seyal Déminéralisée En Milieu Peu Hydraté: Propriétés Structurales, d'hydratation et Physicochimiques.* These de doctorat, SupAgro, 2022.